Int. J. Heat Mass Transfer. Vol. 35, No. 8, pp. 1947–1956, 1992
Printed in Great Britain

0017–9310/92 $5.00 + 0.00

Three-dimensional mixed convection flows in a horizontal annulus with a heated rotating inner circular cylinder

LEI YANG and BAKHTIER FAROUK

Department of Mechanical Engineering and Mechanics, Drexel University, Philadelphia, PA 19104, U.S.A.

(*Received* 13 *June* 1990 *and in final form* 23 *July* 1991)

Abstract—The existence of hydrodynamic instabilities leads to the formation of Taylor vortices in flows in the annulus between two concentric cylinders with one or both cylinders rotating. The study of heat transfer within the rotating enclosure is complex. For horizontal configuration, the buoyancy and the centrifugal effects (created by the heated rotating cylinder) are orthogonal and give rise to fully three-dimensional flows. The results of a three-dimensional numerical analysis of flows and heat transfer in a horizontal annulus with a heated rotating inner circular cylinder are presented. Solutions are presented over a wide range of the rotational Reynolds (Taylor) number and the Grashof number. The effect of the centrifugal instability on the heat transfer is examined. The aspect ratio Γ is varied from 1.0 to 10.0 while the radius ratio η for the annulus is maintained at the value of 2.6 for the results presented.

INTRODUCTION

THE STUDY of heat transfer in rotating bodies has a variety of practical applications in industry. These include cooling of turbine rotors or electrical motor shaft, cooling of high speed gas bearings, rotating condensers for sea water distillation, etc. The flow fields in such systems are complex due to interactions of the inertia, buoyancy and the centrifugal effects. In a heated rotating system the buoyancy and the centrifugal forces are of importance. The resultant combination of these determines the flow pattern and the heat transfer mechanism. Two-dimensional natural convection in a horizontal concentric annulus has been intensely studied numerically and experimentally in both laminar and turbulent regimes [1–5]. The forced flow due to an unheated rotating cylinder, in which only the centrifugal force is considered, will lead to the Taylor vortices because of the existence of hydrodynamic instability when the Reynolds (Taylor) number reaches a critical value [6, 7]. A comprehensive review of the analytical and experimental investigations for the annulus with a rotating inner cylinder is given by DiPrima and Swinney [8]. Ball and Farouk [9] and Ball [10] undertook a detailed study on the development of Taylor vortices and the distribution of heat transfer in a vertical annulus with a heated rotating inner cylinder. For the vertical orientation (for moderate speeds of rotation), the flow field generated by the centrifugal and the buoyancy effects are both axisymmetric. For the horizontal configuration, however, the buoyancy and the centrifugal effects will give rise to fully three-dimensional flows when the centrifugal force is strong enough to trigger the formation of the Taylor cells. Fusegi *et al.* [11] presented numerical results for two-dimensional $(r-\theta)$ mixed convection in the annulus between horizontal concentric cylinders with a heated rotating inner cylinder. The study was limited to slow rotational speeds of the inner cylinder so that the appearance of Taylor cells was precluded. When the rotational Reynolds number is increased beyond a critical value, the flow will become unstable hydrodynamically and will then lead to the formation of Taylor vortices which necessitates a three-dimensional analysis. Fusegi and Farouk [12] also presented results for three-dimensional natural convection within an annulus with an aspect ratio of unity.

This paper presents the results of three-dimensional mixed convection in a horizontal rotating annulus. The main objective of the paper is to quantify the interaction of the buoyancy and centrifugal forces and determine the effects of secondary flow structures (due to the Taylor cells) on the heat transfer. From the heat transfer distributions on the surfaces, the structure of convective flow is evaluated. The inner cylinder is considered to be rotating at a uniform speed while the outer cylinder and end-plates are held stationary. Both the inner and the outer cylinders are isothermal with the inner cylinder being hotter than the outer one. The no-slip conditions are applied for all enclosure surfaces. Thermally insulated flat end-plates are considered. The geometry of the problem is shown in Fig. 1 where the angle θ is measured from the bottom vertical line.

MATHEMATICAL FORMULATION

The geometry is specified by the radius ratio $\eta = R_o/R_i$ and the aspect ratio $\Gamma = H/d$, where d denotes the gap width $(R_o - R_i)$. The aspect ratio is

NOMENCLATURE

d	gap width, $R_o - R_i$
Gr	Grashof number, $g\beta d^3(T_i - T_o)/v^2$
H	height of annulus
k	thermal conductivity
Nu	Nusselt number, $qd/k(T_i - T_o)$
p	pressure
Pr	Prandtl number, $C_p\mu/k$
q	heat flux
r	radius
R	radius of inner or outer cylinder
Re	Reynolds number, $\omega R_i d/v$
t	time
T	temperature
u	radial velocity component
v	angular velocity component
w	axial velocity component
z	axial location.

Greek symbols

Γ	aspect ratio, H/d
η	radius ratio, R_o/R_i
θ	circumferential location
μ	molecular viscosity
ν	kinematic viscosity
σ	densiometric Froude number, Gr/Re^2
ω	angular speed of rotation of inner cylinder.

Subscripts

i	inner cylinder
o	outer cylinder.

varied from 1.0 to 10.0 and the radius ratio is set equal to 2.6 for all cases considered. The wide range of aspect ratio studied revealed interesting effects on the structure of the secondary flow fields. Air is considered as the medium, with the Prandtl number being equal to 0.72.

Governing equations and boundary conditions

Three-dimensional incompressible Navier–Stokes and energy equations were used to describe the problem. By introducing the following dimensionless variables (an overbar means a dimensional quantity)

$$r = \frac{\bar{r}}{d} \quad z = \frac{\bar{z}}{d} \quad u = \frac{\bar{u}}{u_0} \quad v = \frac{\bar{v}}{u_0} \quad w = \frac{\bar{w}}{u_0} \quad t = \frac{\bar{t}u_0}{d}$$

$$p = \frac{\bar{p}}{u_0^2\rho_0} \quad \text{and} \quad T = \frac{\bar{T} - \bar{T}_o}{\bar{T}_i - \bar{T}_o} \quad \text{where} \quad u_0 = \frac{v}{d}$$

the dimensionless time-dependent equations of fluid flow and heat transfer in cylindrical coordinates are given by

$$\frac{1}{r}\frac{\partial}{\partial r}(ru) + \frac{1}{r}\frac{\partial v}{\partial \theta} + \frac{\partial w}{\partial z} = 0 \tag{1}$$

$$\frac{\partial u}{\partial t} + u\frac{\partial u}{\partial r} + \frac{v}{r}\frac{\partial u}{\partial \theta} + w\frac{\partial u}{\partial z} - \frac{v^2}{r} = -\frac{\partial p}{\partial r} + \left(\nabla^2 u - \frac{u}{r^2} - \frac{2}{r^2}\frac{\partial v}{\partial \theta}\right) - Gr\, T\cos(\theta) \tag{2}$$

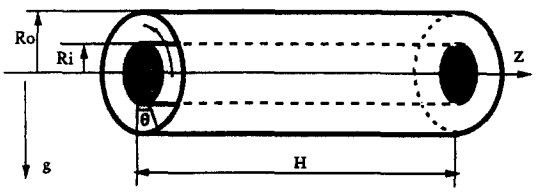

FIG. 1. The three-dimensional annular geometry.

$$\frac{\partial v}{\partial t} + u\frac{\partial v}{\partial r} + \frac{v}{r}\frac{\partial v}{\partial \theta} + \frac{uv}{r} + w\frac{\partial v}{\partial z} = -\frac{1}{r}\frac{\partial p}{\partial \theta} + \left(\nabla^2 v - \frac{v}{r^2} + \frac{2}{r^2}\frac{\partial u}{\partial \theta}\right) + Gr\, T\sin(\theta) \tag{3}$$

$$\frac{\partial w}{\partial t} + u\frac{\partial w}{\partial r} + \frac{v}{r}\frac{\partial w}{\partial \theta} + w\frac{\partial w}{\partial z} = -\frac{\partial p}{\partial z} + \nabla^2 w \tag{4}$$

and

$$\frac{\partial T}{\partial t} + u\frac{\partial T}{\partial r} + \frac{v}{r}\frac{\partial T}{\partial \theta} + w\frac{\partial T}{\partial z} = \frac{1}{Pr}\nabla^2 T. \tag{5}$$

The Boussinesq approximation is applied in the above formulation. The coupled sets of equations are numerically integrated with the following boundary conditions:

along the inner cylinder: ($r = 0.625$)

$$u = 0 \quad v = Re \quad w = 0 \quad T = 1$$

along the outer cylinder ($r = 1.625$)

$$u = 0 \quad v = 0 \quad w = 0 \quad T = 0$$

along the end-plates ($z = 0$ and $z = z_H$)

$$u = 0 \quad v = 0 \quad w = 0 \quad \frac{\partial T}{\partial z} = 0.$$

For the present formulations and the non-dimensional parameters used, the rotational effects enter via the boundary conditions at the inner cylinder. It can be shown easily that the relative strength of the buoyancy and the centrifugal forces in the problem is given by the ratio σ (densiometric Froude number) = Gr/Re^2. For isothermal flows ($Gr = 0.0$), the rotating inner cylinder induces a Couette flow for slow speeds of rotation. The rotational instability (Taylor vortex flow) is triggered when the Reynolds number exceeds a critical value (often described as the critical Taylor number in the literature). When a temperature

gradient exists in the problem, the buoyancy induced flow interacts with the rotational flow which can delay the onset of the Taylor vortex type flow in the annulus.

The Nusselt numbers $Nu\,(z,\theta)$ for the inner and the outer cylinders are defined as

$$Nu\,(z,\theta)_i = q(z,\theta)_i d/[k(T_i - T_o)]$$

and

$$Nu\,(z,\theta)_o = q(z,\theta)_o d/[k(T_i - T_o)],$$

respectively.

For convenience in presenting the results, we define the circumferentially averaged Nusselt number Nu_θ for the inner and outer cylinders as

$$\overline{Nu_\theta} = \frac{1}{2\pi}\int_0^{2\pi} Nu\,(\theta,z)\,\mathrm{d}\theta.$$

Similarly, the longitudinally averaged Nusselt number Nu_z is defined as follows:

$$\overline{Nu_z} = \frac{1}{z_H}\int_0^{z_H} Nu\,(\theta,z)\,\mathrm{d}z$$

where z_H is the length of the annulus. The global mean Nusselt number (for the inner or the outer cylinder) then can be defined as

$$\overline{\overline{Nu}} = \frac{1}{2\pi z_H}\int_0^{2\pi}\int_0^{z_H} Nu\,(\theta,z)\,\mathrm{d}z\,\mathrm{d}\theta.$$

NUMERICAL METHOD

A staggered mesh system is adopted for the derivations and solution of the finite difference approximation to the differential equations. The SIMPLE scheme of Patankar [13] is used to solve the finite difference equations resulting from the discretization. The application of the SIMPLE algorithm in cylindrical coordinates is quite common and the details of the application are given in Patankar [13]. For specified Grashof and Reynolds numbers, the resulting finite difference equations are solved in a time marching manner until a steady state condition is achieved. The computations employ a uniform mesh system with $11(r)\times 24(\theta)\times 30(z)$ grid points for low aspect ratio ($\Gamma < 6.0$) cases. The grid points in the axial directions were proportionately increased for the high aspect ratio cases. For the range of parameters considered and the aspect and radius ratios of the problem geometry, the above grids were found to be adequate. Sample calculations were performed with denser grids for selected cases which did not produce appreciable differences in the flow structure or the heat transfer characteristics. All computations were performed on a CRAY X-MP supercomputer at the Pittsburgh Supercomputing Center. The typical CPU time used for one complete case was about 600 s.

RESULTS AND DISCUSSION

Results were obtained for isothermal ($Gr = 0.0$), non-rotating ($Re = 0.0$) and mixed convection modes for the finite annular geometry. The maximum allowable values of Gr and Re were sufficiently low so that only laminar flows were encountered. While results were obtained for different values of the aspect ratio Γ, the radius ratio η was held constant at 2.6 for all cases considered. For the isothermal case, the flow field is essentially one dimensional (except near the

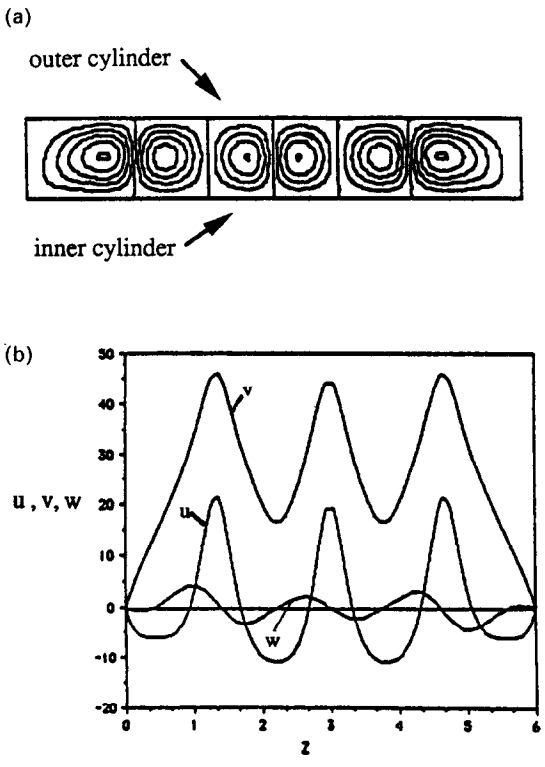

FIG. 2. (a) Streamlines for axisymmetric flow in the finite annulus at any arbitrary θ location $Gr = 0.0$, $Re = 100$, $\Gamma = 6.0$. (b) Velocity distributions along the length of the annulus at $r = (r_o - r_i)/2$ at any arbitrary θ location. $Gr = 0.0$, $Re = 100$, $\Gamma = 6.0$.

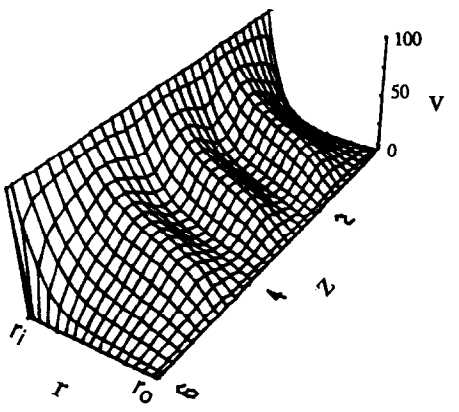

FIG. 3. Azimuthal velocity distribution along the r–z plane at any arbitrary location. $Gr = 0.0$, $Re = 100$, $\Gamma = 6.0$.

end-plates) when the rotational speed of the inner cylinder is below the critical Reynolds number. From linear stability theory, the critical Reynolds number for the onset of the Taylor vortices (for a wide gap case) is equal to 64. This was verified by our computations also. When $Re > 64$, the flow field is characterized by toroidal vortices which appear in the form of counter-rotating cells. The cells usually occur in pairs and for moderate speeds of rotation of the inner cylinder, the flow field remains axisymmetric. Figure 2(a) shows the streamlines (based on the radial and axial components of velocities) along any arbitrary θ location for $Re = 100$ where $\Gamma = 6.0$. To illustrate the relative magnitudes of all three components of velocity in the flow field, we show the axial distribution of the velocity components at $r = (R_o - R_i)/2$ for any arbitrary θ location. The base flow (v distribution) is found to be strongly affected by the secondary (u–w) flow field. The relief plot for the circumferential component of the velocity field along an arbitrary r–z plane is shown in Fig. 3. The effect of the three pairs of the Taylor cells on the base flow is evident. The axial component of the velocity field along the r–θ plane at $z = 0.8$ is displayed in Fig. 4. The presence of a cell is clearly demonstrated at this location as the axial velocity undergoes a change in sign along the radius of the gap width.

A pure natural convective case ($Gr = 1.39 \times 10^4$ and

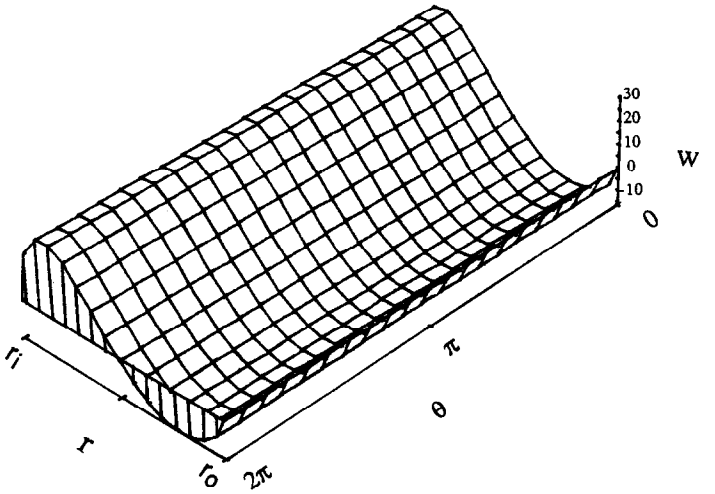

FIG. 4. Axial velocity distribution along r–θ plane at $z = 0.8$. $Gr = 0.0$, $Re = 100$, $\Gamma = 6.0$.

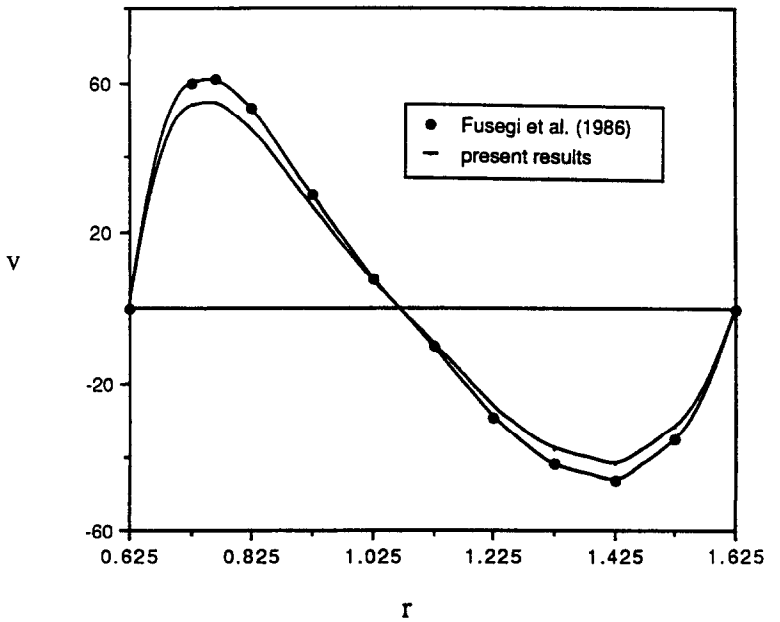

FIG. 5. Azimuthal velocity distribution along the radius at $\theta = 90°$, $z = 0.5\, z_H$ for $Gr = 1.39 \times 10^4$, $Re = 0.0$.

$Re = 0$) is considered next. Figure 5 shows the azimuthal velocity distribution along the radius at $\theta = 90°$ and $z = 0.5\, z_H$. The aspect ratio for the above case is 6.0. The velocity distribution shows the characteristic flow inversion encountered in natural convection flows in a horizontal annulus. Results obtained for an infinitely long horizontal annulus ($\Gamma = \infty$) by Fusegi *et al.* [11] for the same conditions are also shown in Fig. 5. While the present results agree well with the predictions given in ref. [11], the peak values of the velocity predicted for the finite aspect ratio annulus are smaller than those predicted for the infinitely long annulus. This is due to the damping effect of the end-plates considered in the present calculations.

Sets of calculations were then carried out where the Reynolds number was fixed at 100 while the Grashof number was varied from 138 to 6944. The calculations were carried out for three specific values of Γ, i.e. 3.0, 6.0 and 10.0. Detailed results for the cases with $\Gamma = 6.0$ are shown below. Figures 6(a) and (b) show the relief plots of local Nusselt number $Nu\ (z, \theta)$ distribution at the inner and outer cylinder for $Re = 100$ and $Gr = 138$ with $\sigma = 0.014$. The densiometric Froude number σ is quite small, which means that the centrifugal force dominates. The flow pattern is characterized by the appearance of Taylor cells which strongly affects the heat transfer characteristics at the inner cylinder. A strong jet-like flow exists at the

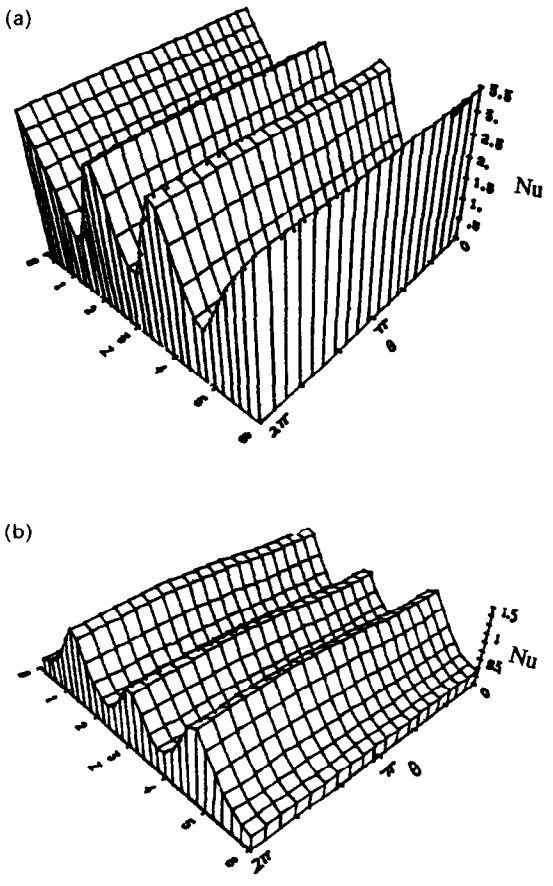

FIG. 6. (a) Local Nusselt number distribution on the inner cylinder. $Re = 100$, $Gr = 138$, $\Gamma = 6.0$. (b) Local Nusselt number distribution on the outer cylinder. $Re = 100$, $Gr = 138$, $\Gamma = 6.0$.

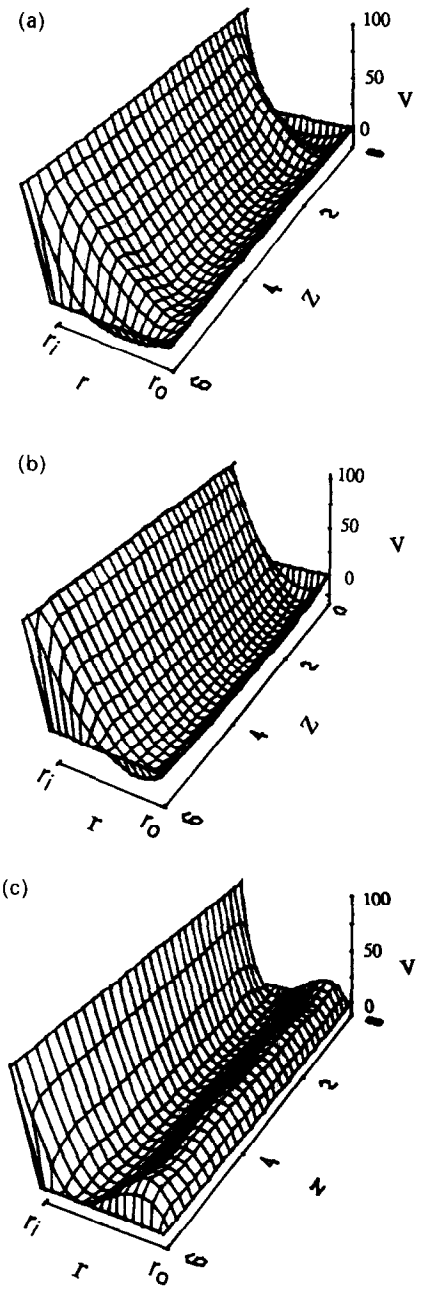

FIG. 7. (a) Azimuthal velocity distribution along the r–z plane at $\theta = 90°$ location. $Re = 100$, $Gr = 138$, $\Gamma = 6.0$. (b) Azimuthal velocity distribution along the r–z plane at $\theta = 180°$ location. $Re = 100$, $Gr = 138$, $\Gamma = 6.0$. (c) Azimuthal velocity distribution along the r–z plane at $\theta = 270°$ location. $Re = 100$, $Gr = 138$, $\Gamma = 6.0$.

demarcation of two counter-rotating cells which results in increased heat transfer at the inner and outer cylinder surfaces [10]. The variation of the Nusselt number is wave-like in the axial direction owing to the regular formation of the Taylor cells. The local heat transfer is, however, almost constant along the circumferential direction. As the surface area of the inner cylinder is larger than that of the outer cylinder, the magnitude of the average Nusselt number on the inner cylinder is larger than that of the outer cylinder. Energy balance calculations resulted in an excellent agreement between the inner and the outer cylinder heat transfers. For the same Re and $\sigma = 0.14$ (results not shown), the wavy nature of the Nusselt number distribution along the axial direction persists, indicating the continued presence of the Taylor cells. The velocity field within the annulus is shown next for the case where $Re = 100$, $Gr = 6944$, and $\sigma = 0.69$. The circumferential velocity component v is shown along the r–z plane at $\theta = 90$, 180 and 270 in Figs. 7(a), (b) and (c), respectively. It is clear from these figures that, at this value of Grashof number, the buoyancy-induced field is strong and the effects of the Taylor cells on the heat transfer are subdued. At this high Grashof number, the critical Reynolds number for the onset of the Taylor cells is higher than 100. We did not attempt to evaluate the value by simulation because at the higher Re steady laminar flow may not be present. The heat transfer results for the above case are shown in Figs. 8(a) and 7(b). For the inner cylinder (Fig. 8(a)), the local heat transfer varies along the circumferential direction only. The shape of the plots looks similar to those found in typical natural convection flow fields in a horizontal annulus. For the outer cylinder (Fig. 8(b)), the Nusselt number peaks near $\theta = \pi$ radians. The flow field near the outer cylinder is vigorous and the effects of two stationary end walls on heat transfer are prominent in Fig. 8(b). For the outer cylinder the heat transfer peaks near the end-plates.

Figures 9(a) and (b) show the distribution of the circumferentially averaged Nusselt number Nu_θ (for the inner and the outer cylinders) along the axial

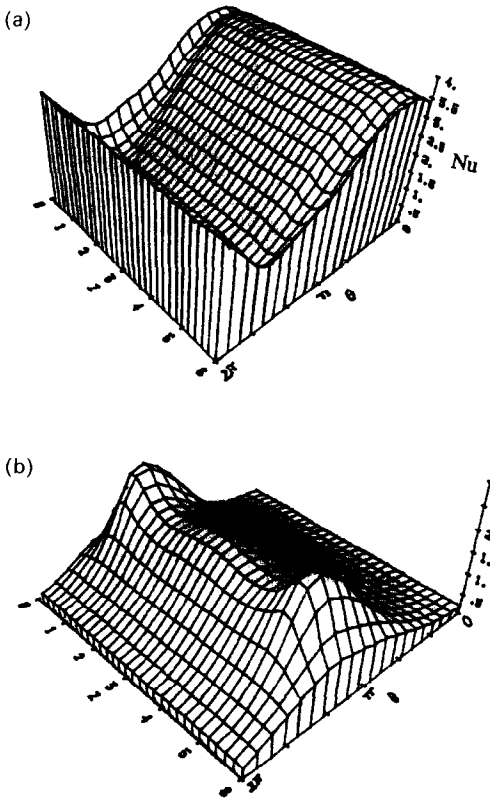

FIG. 8. (a) Local Nusselt number distribution on the inner cylinder. $Re = 100$, $Gr = 6944$, $\Gamma = 6.0$. (b) Local Nusselt number distribution on the outer cylinder. $Re = 100$, $Gr = 6944$, $\Gamma = 6.0$.

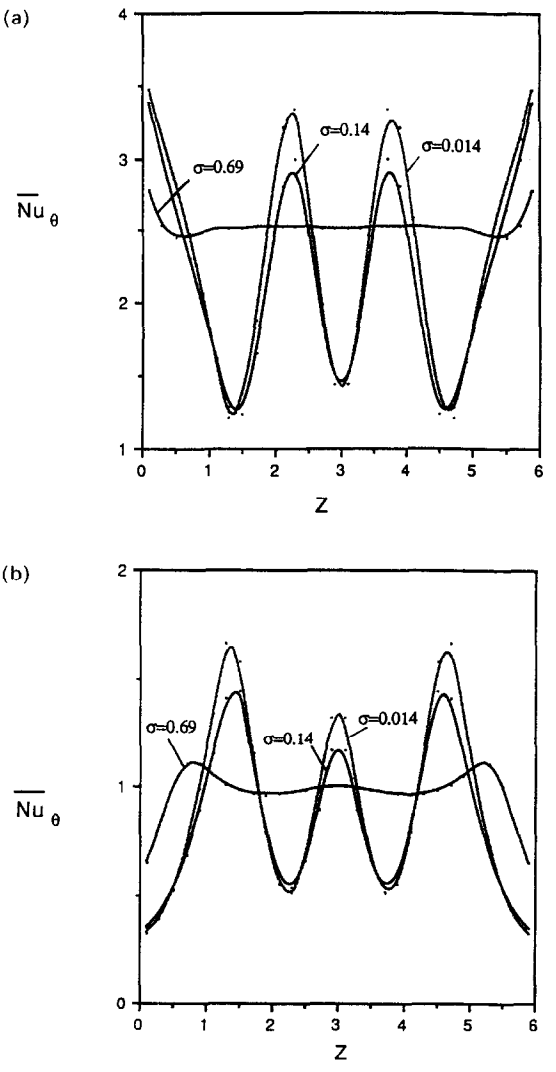

FIG. 9. (a) Circumferentially averaged Nusselt number, Nu_θ, distribution for the inner cylinder. $Re = 100$, $\Gamma = 6.0$, $Gr = 138$, 1388, 6944. (b) Circumferentially averaged Nusselt number, Nu_θ, distribution for the outer cylinder. $Re = 100$, $\Gamma = 6.0$, $Gr = 138$, 1388, 6944.

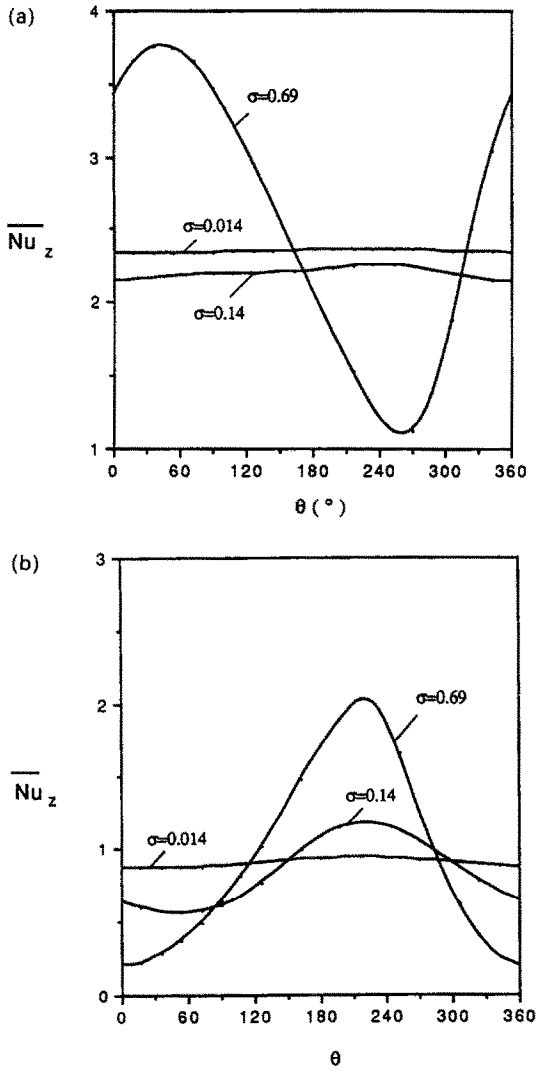

FIG. 10. (a) Axially averaged Nusselt number, Nu_z, distribution for the inner cylinder. $Re = 100$, $\Gamma = 6.0$, $Gr = 138$, 1388, 6944. (b) Axially averaged Nusselt number, Nu_z, distribution for the outer cylinder. $Re = 100$, $\Gamma = 6.0$, $Gr = 138$, 1388, 6944.

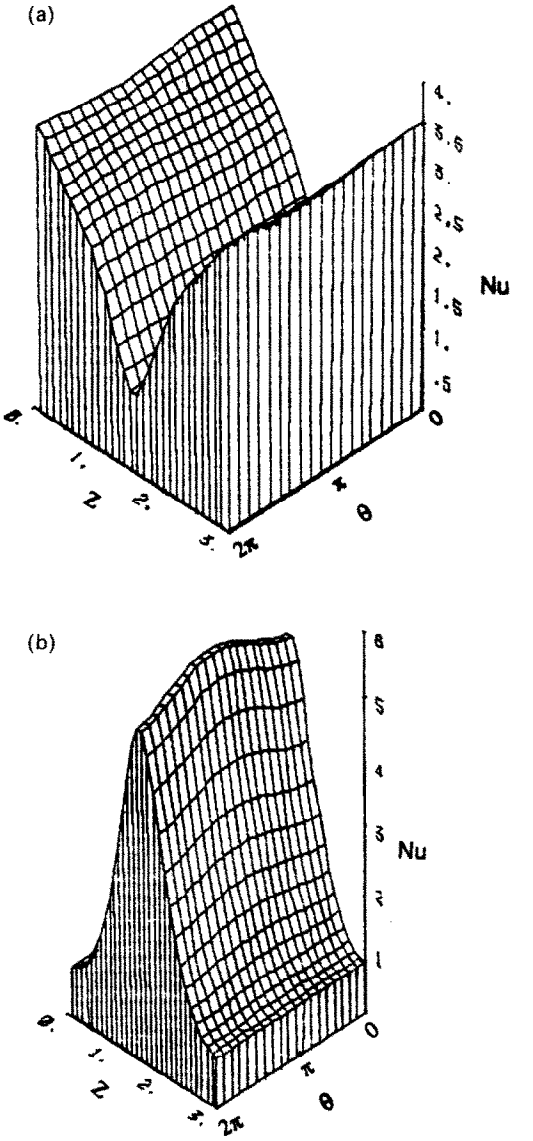

FIG. 11. (a) Local Nusselt number distribution on the inner cylinder. $Re = 100$, $Gr = 138$, $\Gamma = 3.0$. (b) Local Nusselt number distribution on the outer cylinder. $Re = 100$, $Gr = 138$, $\Gamma = 3.0$.

direction for the cases where $\Gamma = 6$, $Re = 100$ and $\sigma = 0.014$, 0.14 and 0.69, respectively. Figures 10(a) and (b) show the Nu_z distribution along the θ direction (for the inner and the outer cylinders) for the above cases. The circumferential averaging provides the general information along the axial direction while Nu_z shows the overall heat transfer variation along the θ direction. It can be seen from Figs. 9(a) and (b) that for $\sigma = 0.014$, which is the rotation dominated case, that Nu_θ fluctuates along the axial direction according to the distribution of the Taylor vortices. In Figs. 10(a) and (b), Nu_z appears as a flat line for $\sigma = 0.014$. For $\sigma = 0.69$, which is a buoyancy dominated case, the Nu_z changes significantly with θ while the Nu_θ variations in Figs. 9(a) and (b) look rather flat. The effect of the Taylor cells on the heat transfer is prominent for small values of σ. It is interesting to note that the buoyancy effects dominate well before σ reaches a value of unity.

Results are presented next for heat transfer in shorter annuli. Figures 11(a) and (b) show the local Nusselt number distributions along the inner and the outer cylinders for $Re = 100$, $Gr = 138$ and $\Gamma = 3.0$. From the profiles, it is evident that only one pair of Taylor cells is formed as opposed to three for the similar case with $\Gamma = 6.0$. Figures 12(a) and (b) show the heat transfer results for $\Gamma = 1.0$ where the other parameters were the same as before. The Nusselt number values are substantially smaller due to the insulated end caps, however, a pair of Taylor cells is still evident.

In Fig. 13, the variation of the mean global heat

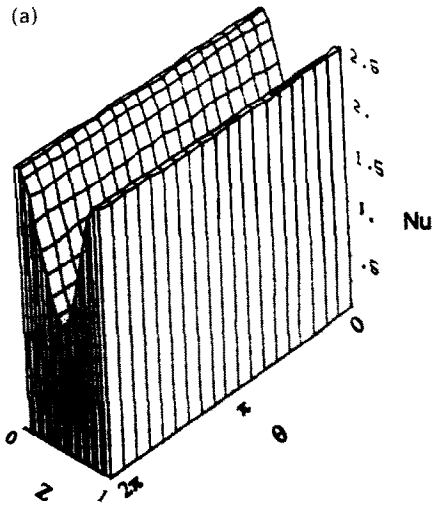

FIG. 12. (a) Local Nusselt number distribution on the inner cylinder. $Re = 100$, $Gr = 138$, $\Gamma = 1.0$. (b) Local Nusselt number distribution on the outer cylinder. $Re = 100$, $Gr = 138$, $\Gamma = 1.0$.

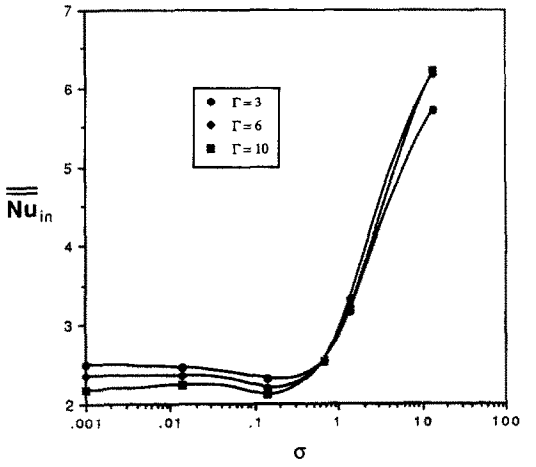

FIG. 13. Global mean Nusselt number as a function of $\sigma(Gr/Re^2)$ for $Re = 100$ for three different aspect ratios.

transfer at the inner cylinder as a function of σ (at $Re = 100$) is shown for three different aspect ratios. All three curves show minima values indicating the opposing effects of the buoyant and rotational flows. When σ is between 0.1 and 0.3, the Taylor cells and the developing buoyancy-induced flow fields appear to have a cumulative destructive effect on the heat transfer. A steady increase is shown in heat transfer with increasing values of σ when the flow becomes buoyancy dominated. For the rotation dominated cases, the global heat transfer was found to decrease slightly with increasing aspect ratio. For the buoyancy dominated cases, the trend was found to be reversed. However, no generalization can be made as these trends can depend on the Re itself (presence of secondary flow, turbulence, etc.).

Figure 14 shows the global heat transfer as a function of the aspect ratio for two values of σ with $Re = 100$. Interesting features are observed in this figure. For all cases, the heat transfer drops off sharply as the aspect ratio is decreased. For rotation and dominated cases, heat transfer is found to attain the maximum value when Γ is between 3 and 4. For larger aspect ratios, the buoyancy dominated case reaches an asymptote. However, the rotation dominated case continues to show a slow decrease in heat transfer as the aspect ratio is increased. However, for even larger aspect ratios (than those considered in Fig. 14), the heat transfer will reach an invariant value.

A limited study was carried out to investigate the effects of rotation on the heat transfer as the Gr and Γ values were held constant. Figures 15 and 16 present the distribution of averaged Nusselt numbers Nu_θ and Nu_z along the axial and circumferential directions for the inner cylinder where Gr and Γ are held fixed at 2777 and 6.0, respectively, and the rotational speed of

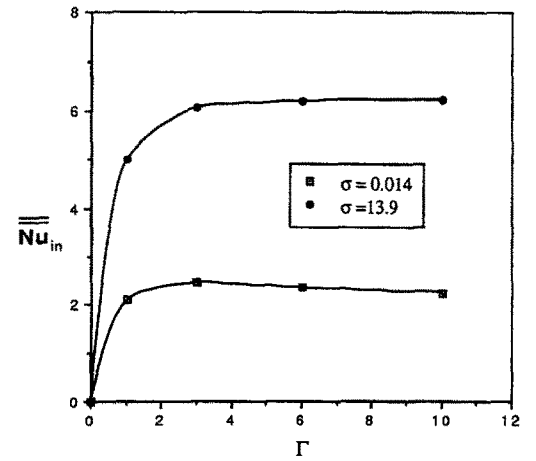

FIG. 14. Global mean Nusselt number as a function of the aspect ratio for $Re = 100$ and two different values of $\sigma(Gr/Re^2)$.

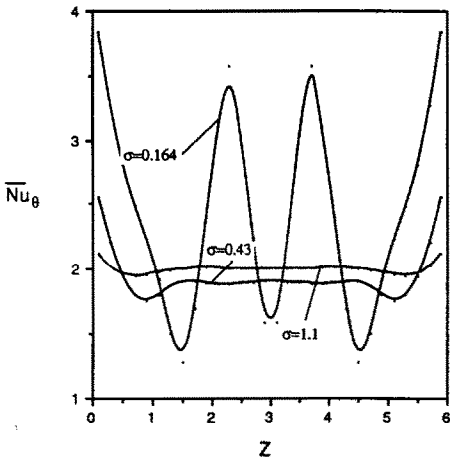

FIG. 15. Circumferentially averaged Nusselt number, Nu_θ, distribution for the inner cylinder. $Gr = 2777$, $\Gamma = 6.0$, $Re = 50, 80, 130$.

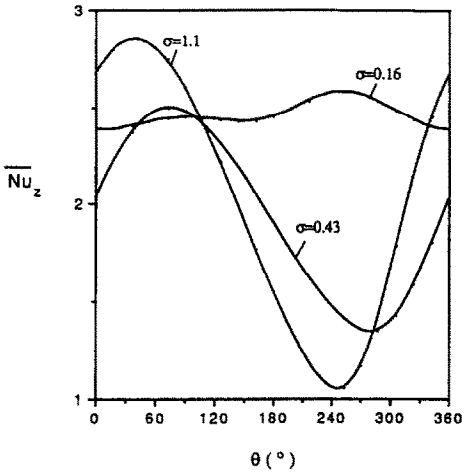

FIG. 16. Axially averaged Nusselt number, Nu_z, distribution for the inner cylinder. $Gr = 2777$, $\Gamma = 6.0$, $Re = 50, 80, 130$.

the inner cylinder is varied ($\sigma = 0.164$, 0.43 and 1.1). The corresponding results for the outer cylinder are not shown for the sake of brevity. Figure 15 shows that when σ is small (high Re), the presence of the Taylor cells considerably augments the heat transfer. When $Gr = 2777$ and $Re = 80$, the flow is still found to be buoyancy dominated as seen in Fig. 16. From our calculations, at this Gr, the onset of rotational instability occurs somewhere between $Re = 80$ and 130. As discussed earlier, from the linear stability theory, the critical Reynolds number for the onset of the Taylor vortices for the isothermal problem is 64. The natural convection flow field (which is well developed at $Gr = 2777$) thus inhibits and delays the formation of the Taylor cells. From Fig. 16 it is seen that the azimuthal variation becomes important when the buoyancy effects dominate. The peak heat transfer in the stationary inner cylinder occurs at the 0° location. The location shifts towards higher θ values as the rotational speed of the inner cylinder increases.

CONCLUSIONS

In this paper, the interaction of centrifugal and buoyancy forces has been studied in a finite horizontal annulus with a heated rotating inner cylinder. The resulting flows are fully three dimensional for cases where the rotational instability triggers the formation of Taylor cells. Owing to the existence of the buoyancy force, the critical Reynolds (Taylor) number value will be higher for the heated rotating inner cylinder. The radius ratio of the annulus was held fixed for the calculations, but the effect of the aspect ratio on the flow field and heat transfer was explored. These effects were investigated in detail for $Re = 100$ (sufficient to trigger secondary flows in an isothermal annulus) as the Gr and σ were varied systematically. A limited study was also carried out where Gr and Γ were held fixed at 2777 and 6.0, respectively, and the Re values were varied.

In rotation dominated cases, for $\eta = 2.6$, the global heat transfer attains the maximum value when the aspect ratio is between 3.0 and 4.0. Three pairs of cells are observed within the annulus for the range of the Reynolds number considered. In the buoyancy dominated cases, the global heat transfer increases with the aspect ratio and reaches an asymptote (equivalent two-dimensional solution).

Acknowledgement—The authors gratefully acknowledge the computational resources provided by the Pittsburgh Supercomputing Center (Grant No. 880027P).

REFERENCES

1. C. Y. Liu, W. K. Mueller and F. Landis, Numerical convection heat transfer in long horizontal annuli, *Int. Dev. Heat Transfer, ASME* 976–984 (1961).
2. J. Lis, Experiment investigation of natural convection heat transfer in simple and obstructed horizontal annuli, *Proc. 3rd Int. Heat Transfer Conf.*, Vol. 2, pp. 196–204 (1966).
3. T. H. Kuehn and R. J. Goldstein, An experimental and theoretical study of natural convection in the annulus between horizontal concentric annulus, *J. Fluid Mech.* **75,** 695–719 (1976).
4. P. F. Hodnett, Natural convection between horizontal heated concentric circular cylinders, *J. Appl. Math. Phys.* **24,** 507–516 (1973).
5. B. Farouk and S. I. Guceri, Laminar and turbulent natural convection in the annulus between horizontal concentric cylinders, *ASME J. Heat Transfer* **104,** 631–636 (1982).
6. G. I. Taylor, Stability of viscous liquid contained between two rotating cylinders, *Phil. Trans. Soc. A* **223,** 289–343 (1923).
7. D. Coles, Transition in circular Couette flow, *J. Fluid Mech.* **21,** 385–425 (1965).
8. R. C. DiPrima and H. L. Swinney, Instabilities and transition in flow between concentric rotating cylinders. In *Hydrodynamic Instabilities and the Transition to Tur-*

bulence (Edited by H. L. Swinney and J. P. Gollub), pp. 139–186. Springer, New York (1985).
9. K. S. Ball and B. Farouk, On the development of Taylor vortices in a vertical annulus with a heated rotating inner cylinder, *Int. J. Numer. Meth. Fluids* **7**, 857–867 (1987).
10. K. S. Ball, Mixed convection heat transfer in rotating system, Ph.D. thesis, Department of Mechanical Engineering and Mechanics, Drexel University (1987).
11. T. Fusegi, B. Farouk and K. S. Ball, Mixed convection flows within a horizontal concentric annulus with a heated rotating inner cylinder, *Numer. Heat Transfer* **9**, 591–604 (1986).
12. T. Fusegi and B. Farouk, A three-dimensional study of natural convection in the annulus in between horizontal concentric cylinders, *Eighth Int. Heat Transfer Conf.*, San Francisco, CA, pp. 1575–1579. Hemisphere, New York (1986).
13. S. V. Patankar, *Numerical Heat Transfer and Fluid Flow*, pp. 113–131. McGraw-Hill, New York (1980).

ECOULEMENTS DE CONVECTION MIXTE TRIDIMENSIONNELLE DANS UN ESPACE ANNULAIRE HORIZONTAL AVEC LE CYLINDRE CIRCULAIRE INTERIEUR TOURNANT

Résumé—L'existence d'instabilités hydrodynamiques pour des écoulements dans l'espace annulaire entre deux cylindres concentriques avec un ou deux cylindres tournants conduit à la formation des tourbillons de Taylor. L'étude du transfert thermique associé est complexe. Pour la configuration horizontale, les effets de flottement et de centrifugation (due à la rotation du cylindre) sont orthogonaux et donnent naissance à des écoulements tridimensionnels. On présente les résultats d'une analyse tridimensionnelle numérique de l'écoulement et du transfert de chaleur avec le cylindre interne chaud et rotatif, pour des larges domaines de nombres de Reynolds (Taylor) et de Grashof. On examine l'effet de l'instabilité centrifuge sur le transfert thermique. Le rapport de forme Γ varie de 1,0 à 10,0 tandis que le rapport des rayons η est maintenu à la valeur de 2,6 pour les résultats présentés.

DREIDIMENSIONALE MISCHKONVEKTION IN EINEM WAAGERECHTEN RINGSPALT MIT BEHEIZTEM UND ROTIERENDEM INNEREM ZYLINDER

Zusammenfassung—Die Existenz hydrodynamischer Instabilitäten führt zur Bildung von Taylor-Wirbeln in der Strömung im Ringraum zwischen zwei konzentrischen Zylindern, von denen entweder einer oder beide rotieren. Die Untersuchung des Wärmetransports innerhalb des rotierenden Hohlraums ist sehr kompliziert. Bei waagerechter Anordnung stehen die Auftriebswirkung und die Zentrifugalwirkung (hervorgerufen durch den beheizten rotierenden Zylinder) zueinander senkrecht und führen zu einer vollständig dreidimensionalen Strömung. Es werden die Ergebnisse einer dreidimensionalen numerischen Untersuchung von Strömung und Wärmetransport in einem waagerechten Ringspalt mit beheiztem rotierendem innerem Kreiszylinder vorgestellt. Dies geschieht für einen weiten Bereich der Rotations-Reynolds-(Taylor) Zahl und der Grashof-Zahl. Der Einfluß der Zentrifugal-Instabilität auf den Wärmetransport wird überprüft. Das Seitenverhältnis Γ wird zwischen 1,0 und 10,0 variiert, während das Radienverhältnis η des Ringspaltes konstant den Wert 2,6 behält.

ТРЕХМЕРНЫЕ ТЕЧЕНИЯ ПРИ СМЕШАННОЙ КОНВЕКЦИИ В ГОРИЗОНТАЛЬНОМ КОЛЬЦЕВОМ КАНАЛЕ С НАГРЕТЫМ ВРАЩАЮЩИМСЯ ВНУТРЕННИМ КРУГОВЫМ ЦИЛИНДРОМ

Аннотация—Наличие гидродинамических неустойчивостей приводит к образованию вихрей Тэйлора в течениях по кольцевому каналу мехду двумя концентрическими цилиндрами, один из которых или оба вращаются. Исследование теплопереноса во вращающейся полости является сложной задачей. При горизонтальной конфигурации эффекты подъемных и центробежных сил (создаваемых нагретым вращающимся цилиндром) ортогональны и вызывают полностью развитые пространственные течения. Представлены результаты трехмерного численного анализа течений и теплопереноса в горизонтальном кольцевом канале с нагретым вращающимся внутренним круговым цилиндром. Получены решения для широкого интервала изменений вращательного числа Рейнольдса (Тэйлора) и числа Грасгофа. Определяется влияние центробежной неустойчивости на теплоперенос. Результаты представлены для отношения сторон Γ, изменяющегося от 1,0 до 10,0, и отношения радиусов η кольцевого канала, составляющего 2,6.